Journal of Alloys and Compounds 521 (2012) 39–44

Contents lists available at SciVerse ScienceDirect

Journal of Alloys and Compounds

journal homepage: www.elsevier.com/locate/jallcom

Fe_3O_4—C open hollow sphere assembled by nanocrystals and its application in lithium ion battery

Weidong Zhang, Xiaoya Wang, Henghui Zhou*, Jitao Chen, Xinxiang Zhang

College of Chemistry and Molecular Engineering, Peking University, Beijing 100871, People's Republic of China

ARTICLE INFO

Article history:
Received 7 November 2011
Received in revised form
29 December 2011
Accepted 31 December 2011
Available online 9 January 2012

Keywords:
Lithium ion battery
Anode
Open hollow sphere
Nanocrystal

ABSTRACT

This article reports a solvothermal method to fabricate sub-micrometer hematite α-Fe_2O_3 hollow sphere, and Fe_3O_4—C sphere is obtained with further carbothermal reduction process. The key trick of the solvothermal method is to use crystal water of the raw material $Fe(NO_3)_3{\cdot}9H_2O$ as the water phase in the water/oil "micro-reactor" system. Interestingly, one hole is found on the surface of almost each α-Fe_2O_3/Fe_3O_4 hollow sphere. The obtained material is characterized by X-ray diffraction, scanning electron microscopy, transmission electron microscopy, Brunauer–Emmer–Teller analysis, elemental analysis and its electrochemical properties are also studied. This Fe_3O_4—C composite material shows a high reversible capacity of 917.3 mAh g^{-1} at 90 mA g^{-1}, 849.3 mAh g^{-1} at 900 mA g^{-1}, and can be employed as excellent anode material for high energy-density lithium ion battery.

1. Introduction

In the last two decades with the increasing demand in the electronic market, many research groups are engaged in developing secondary lithium ion battery and its electrode materials [1]. In order to improve the lithium ion battery performance, new electrode materials with high specific capacities are necessary. Recently, transition metal oxides (M_xO_y, M = Fe, Co, Ni, Cu, etc.) show remarkable specific capacities about 600 mAh g^{-1} (for example, 928 mAh g^{-1} for Fe_3O_4 material) [2], much larger than that of the conventional graphite anode material (372 mAh g^{-1}) [3], which make them next generation promising anode materials for high energy-density lithium ion battery.

To deal with the poor lithium ion diffusion in electrode materials which greatly affects the electrochemical performance, many approaches have been employed, such as carbon coating [4–9], nanostructure [10–12], and modified by electronically conductive phases [13–15]. Wan and co-workers [5] synthesized carbon-coated Fe_3O_4 nanospindles with high reversible capacity (~745 mAh g^{-1} at C/5 and ~600 mAh g^{-1} at C/2). Wexler and co-workers [16] obtained Fe_3O_4—C composite nanorods exhibiting ~400 mAh g^{-1} after 100 cycles. And Kim and co-workers [17] reported that Fe–Fe_3O_4 composite nanostructure material release a charge/discharge capacity of about 600 mAh g^{-1} after 50 cycles. Above all, these methods make Fe_3O_4 or its composites more suitable for high energy-density lithium ion battery. However, its poor high-rate performance has not been greatly improved, and more work need to be carried out.

Herein, we fabricated Fe_3O_4—C sub-micrometer open hollow sphere as superior anode material for lithium ion battery by the combination of solvothermal method and carbothermal reduction process. The open hollow sphere is self-assembled with nanoparticles (about 20 nm in diameter) covered with amorphous carbon shells, which improve the electronic conductivity and act as barriers to protect the inner materials as well as maintain their high specific capacity. In this experiment, the obtained Fe_3O_4—C open hollow sphere composite material exhibits excellent capacity retention and outstanding rate performance.

Morphology of the Fe_3O_4—C open hollow sphere composite material was characterized by means of scanning electron microscope (SEM), transmission electron microscope (TEM), X-ray diffraction (XRD), elemental analysis and electrochemical experiments to understand the unique properties of the Fe_3O_4—C open hollow sphere composite material.

2. Experimental details

2.1. Synthesis of anode material

Fe_2O_3 open hollow sphere was synthesized through the solvothermal method. The starting materials were $Fe(NO_3)_3{\cdot}9H_2O$ (99.5% Beijing Chemical Works), sodium dodecyl sulfate (SDS, Sinopharm Chemical Reagent Co., Ltd), N,N′-dimethylformamide (DMF, 99.5% Beijing Chemical Works), hexadecyltrimethyl ammonium (CTAB, Sinopharm Chemical Reagent Co., Ltd.), urea (99% Beijing Chemical Works) and ethylene glycol (Beijing Chemical Works). In a typical synthesis, $Fe(NO_3)_3{\cdot}9H_2O$ (1.404 g) was dissolved in DMF (160 mL) to form a clear solution.

* Corresponding author. Tel.: +86 10 62757908; fax: +86 10 62757908.
E-mail address: hhzhou@pku.edu.cn (H. Zhou).

0925-8388/$ – see front matter © 2012 Elsevier B.V. All rights reserved.
doi:10.1016/j.jallcom.2011.12.172

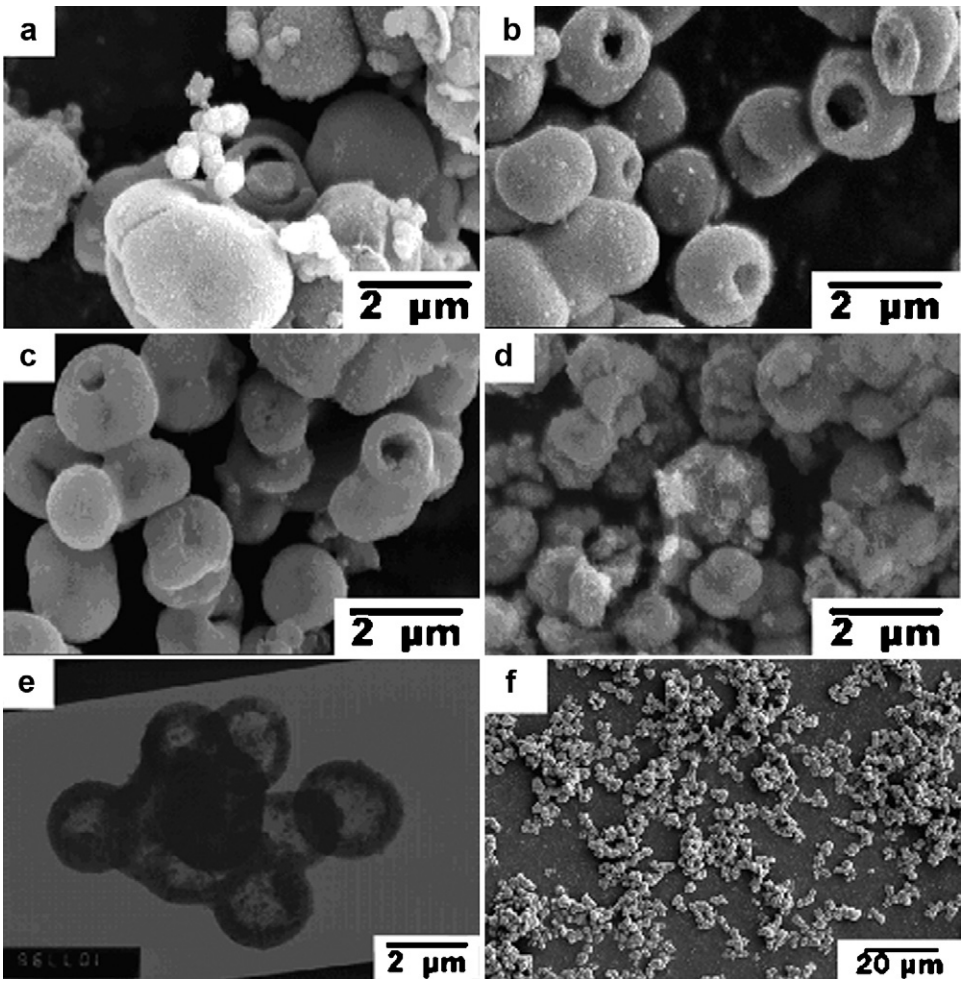

Fig. 1. SEM images of the sample with different urea additions: (a) 0 g, (b) 0.6 g, (c) 1.2 g and (d) 1.8 g. (e) and (f) are TEM image and overall SEM of the sample in (b).

CTAB (0.333 g) and SDS (1.008 g) were added into above solution with vigorous stirring. After 0.5 h, the solution became transparent with CTAB and SDS completely dissolved. Then urea (0.6 g) and ethylene glycol (2 mL) were added into above solution. The obtained solution was sealed in a teflonlined stainless-steel autoclave (50 mL capacity). Then the autoclave was maintained at 150 °C for 12 h, and allowed to cool down to room temperature naturally. The mahogany precipitate was washed by deionized water/ethanol for several times and vacuum-dried at 50 °C for 8 h. In order to get Fe_3O_4—C, the mahogany precipitate was calcined under nitrogen atmosphere in two consecutive steps: at 50 °C for 0.5 h and 550 °C for 0.5 h.

2.2. Characterization of synthesized materials

The morphologies of the as prepared Fe_2O_3 and Fe_3O_4—C materials were characterized by scanning electron microscope (SEM, Hitachi-530) and transmission electron microscope (TEM, JEOL JEM-2010). N_2 adsorption/desorption isotherms were carried out using a Micromeritics ASAP 2010 (USA) analyzer at liquid nitrogen temperature.

Crystal structure of the Fe_2O_3 and Fe_3O_4—C materials were characterized by X-ray scatting (XRD) carried out on Bruker D8 Advance X-ray diffractometer with Cu Kα radiation (λ = 1.5405 Å). And carbon content of the Fe_3O_4—C material was obtained by elemental analysis. X-ray photoelectron energy spectra (XPS) were recorded using monochromatic AlK (1286.6 eV) X-ray sources with 30 eV pass energy in 0.5 eV step over an area of 650 μm × 650 μm to the sample.

2.3. Electrochemical evaluation

To prepare the anode electrode, polyvinylidene difluoride (PVDF, Alfa) was dissolved in N-methylpyrrolidinone (NMP), and then Fe_3O_4—C and super-P carbon black (Alfa) were added (Fe_3O_4—C, super-P and PVDF were mixed in 80:10:10, w/w) and the solution changed into slurry. The slurry was cast on the copper foil and dried at 120 °C under vacuum for 8 h. Then the film was pressed at a pressure of about 10 MPa and punched into round disks with 12 mm in diameter for further experiments.

Standard 2032 coin cell was assembled in a dry Ar-filled glove box to test the electrochemical properties of the Fe_3O_4—C material. Lithium metal foil was used as the counter electrode and 1 M $LiPF_6$ in EC/EMC/DEC (1:1:1, v/v) as the liquid electrolyte. A Celgard 2400 microporous polypropylene membrane was used as the separator. After aging for 4 h, the cell was charged and discharged in the voltage range between 0.5 V and 3.0 V at a current density of 0.1C (900 mAh g^{-1} was assumed to be the 1C rate current) and 1C for 30 cycles. The rate capability was measured by charging at 0.1C current and then discharging at different current densities: 0.2C, 0.5C, 1C and 2C.

3. Results and discussion

The sub-micrometer α-Fe_2O_3 open hollow sphere was fabricated with a solvothermal method including a water/oil "micro-reactor" system. In this system, DMF served as the oil phase, crystal water of $Fe(NO_3)_3{\cdot}9H_2O$ as the water phase, CTAB and SDS as surfactants and carbon sources, urea as OH^- provider [18–20] respectively. Fe_3O_4—C sphere was obtained with further carbon reduce process.

3.1. Structure and morphology evolution of the Fe_2O_3 open hollow sphere

Morphology evolution of Fe_2O_3 open hollow sphere material with the amount of urea added into the solvothermal system is shown in Fig. 1. For the first case that there is no urea as shown in Fig. 1a, the product shows multiple morphologies including particle, hollow sphere, etc. With the increment of urea addition to 0.6 g in Fig. 1b, the as prepared material shows uniform hollow

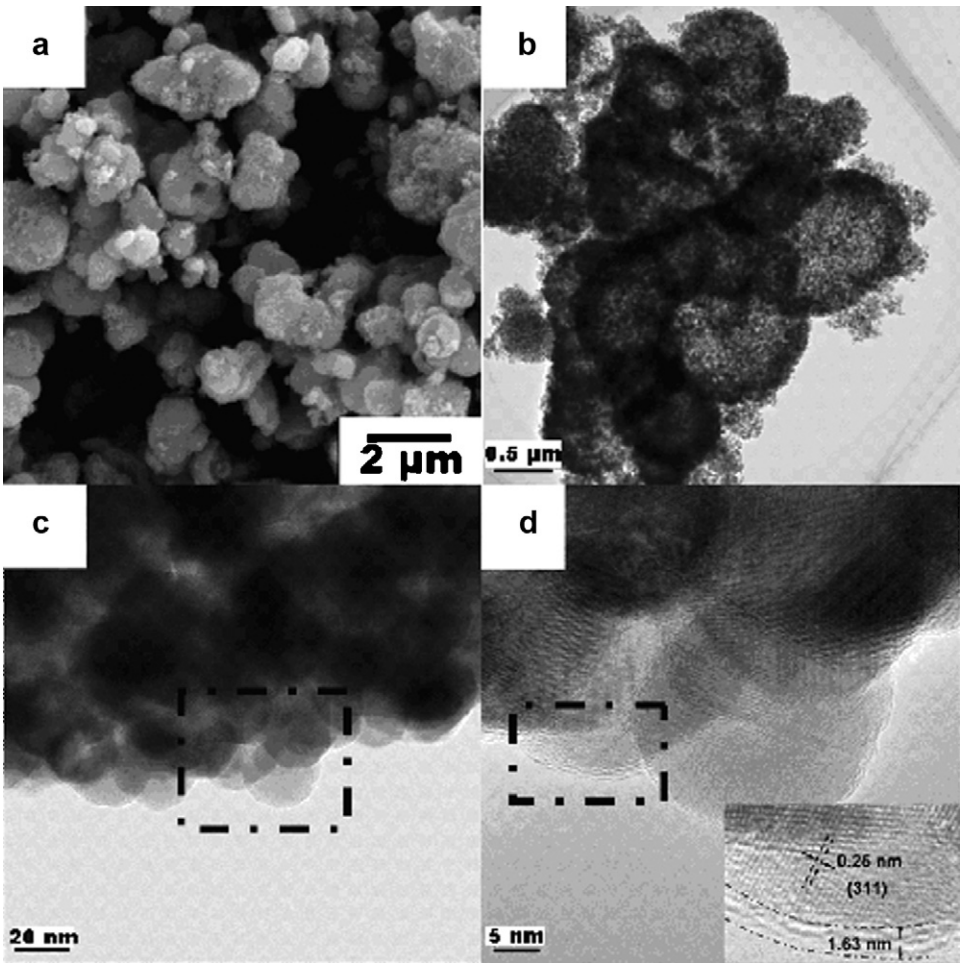

Fig. 2. (a) SEM and (b and c) TEM images of Fe_3O_4—C micrometer open hollow sphere. And (d) HRTEM image from the sample (c) (inset is high magnification image).

sphere morphology with the diameter of 2 μm. And an interesting thing should be noted that there is a hole (about 70 nm in diameter) on the surface of each hollow sphere. This morphology might be induced by the micelle state under these CTAB and SDS contents in the water/oil "micro-reactor", which should be studied for more detailed information in the future. When the urea addition comes up to 1.2 g shown in Fig. 1c, the product has the similar morphology to the sample in Fig. 1b, except for the hole diameter decreases to about 50 nm. With urea addition further increased to 1.8 g in Fig. 1d, a composite of particle and hollow sphere with coarse surface can only be obtained.

In order to investigate the microstructure of the representative sample of Fig. 1b in more detail, TEM is carried out. Fig. 1e shows a TEM image of the sample in Fig. 1b, which reveals that the as-prepared Fe_2O_3 open hollow sphere has the diameter of 2 μm and the wall thickness of about 200 nm from about 20 measurements on the TEM image using the computer software SemAfore 4.0. Fig. 1f shows an overall plan view SEM image of the sample, Fig. 1b, which reveals that the uniform product is well dispersed with high yield ratio as 95%.

3.2. Structure and morphology of the Fe_3O_4—C micrometer open hollow sphere

Fig. 2 shows typical SEM and TEM images of the products of Fe_3O_4—C micrometer open hollow sphere material. It can be seen from Fig. 2a that the Fe_3O_4—C composite material also has open hollow sphere morphology in shape with 1.5 μm in diameter. Formation yield of Fe_3O_4—C micrometer open hollow sphere is as high as 80%. TEM image in Fig. 2b confirms that Fe_3O_4—C micrometer composite material has hollow sphere morphology with an average diameter of ~1.5 μm and an average wall thickness of ~203 nm from about 20 measurements in the TEM image. Compared with the smooth surface of as-prepared Fe_2O_3 open hollow sphere (see Fig. 1b and c), it is noted from Fig. 2a and b that some tiny particles are located on the Fe_3O_4—C micrometer open hollow sphere. They are created during the carbothermal process. The HRTEM image (Fig. 2c) taken on an edge of Fe_3O_4—C micrometer open hollow sphere shows that the sample is assembled by Fe_3O_4 nanocrystals with the diameter of 20 nm. Fig. 2d displays crystal planes with a *d*-spacing of 0.25 nm, corresponding to the (3 1 1) plane of Fe_3O_4. In addition, it is clearly seen from the HRTEM image that an amorphous carbon coating with an average thickness of 1.63 nm covered the Fe_3O_4 nanocrystals. And according to elemental analysis, the carbon content of Fe_3O_4—C composite is 1.97 wt%.

In order to clarify the effect of carbothermal temperature on the as-obtained material structure, XRD experiments are carried out. Fig. 3 shows the XRD patterns of the as-obtained Fe_3O_4—C micrometer open hollow sphere materials under different carbothermal reaction temperatures. When the temperature comes to 350 °C in Fig. 3a, there are only two broad peaks centered at $2\theta = 35.38°$ and 62.46°. As the temperature increases to 450 °C shown in Fig. 3b, the peaks are characteristic of magnetite Fe_3O_4 and all the diffraction peaks could be indexed to spinel phase Fe_3O_4 (JCPDS 86-1354) with cell constant of $a = 0.8440$ nm [21,22]. When the temperature

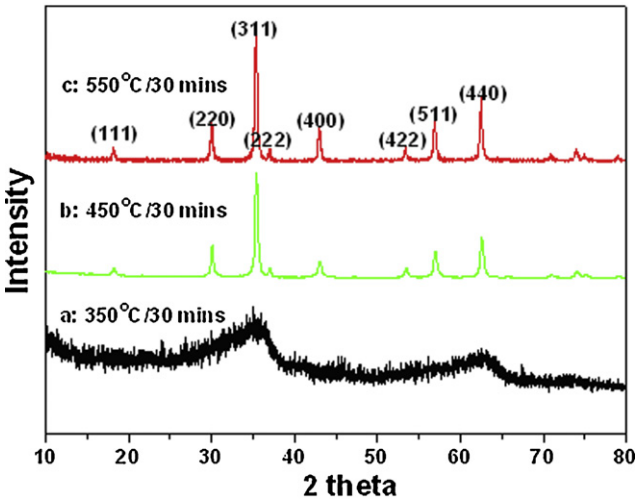

Fig. 3. XRD patterns of the samples obtained under different temperatures: (a) 350 °C, (b) 450 °C, and (c) 550 °C for 30 min.

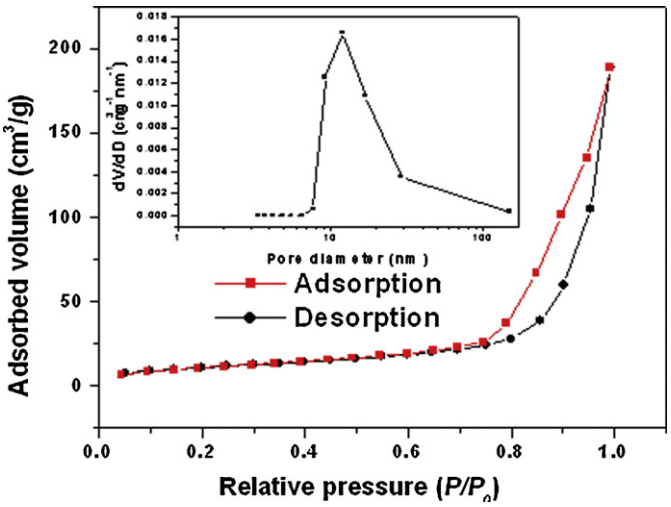

Fig. 5. Nitrogen adsorption–desorption isotherms at 77 K with corresponding BJH desorption pore size distributions (inset).

increases to 550 °C as seen in Fig. 3c, a pure phase of Fe_3O_4 with high crystallinity is obtained. And no obvious XRD peaks corresponding to carbon material are found, indicating the carbon coatings are not well crystallized or smaller than that of detection limit. It should to be noted here that the γ-Fe_2O_3 material has similar XRD patterns to Fe_3O_4 material. Since XPS is a powerful tool to determine the valence of ferric oxides, the Fe_3O_4—C micrometer open hollow sphere material was measured by XPS [see Fig. 4] in order to further confirm the existence of Fe_3O_4. As shown in Fig. 4(inset), the binding energies of $Fe2p_{3/2}$ composed of 711.7 eV and 710.4 eV, which are the characteristic oxidation state of Fe in Fe_3O_4 [23]. And the XPS data also conforms that there is C in the Fe_3O_4—C composite. With the aforementioned results, we choose the Fe_3O_4—C product under 550 °C to carry out further experiments.

Fig. 5 shows the nitrogen adsorption–desorption isotherm and the corresponding Barrett–Joyner–Halenda (BJH) desorption pore size distributions of the as prepared Fe_3O_4—C open hollow sphere. The isotherm feature hysteresis has a well-defined step for the relative pressure P/P_0 ranging from 0.7 to 0.9 between the desorption and adsorption branches, indicating the sample as a characteristic mesoporous material [24]. According to the BJH analysis (inset), the pore size distribution of Fe_3O_4—C micrometer hollow sphere is in the range 12 nm, which are helpful to buffer the volume expansion during Li insertion [6,21]. And BET surface area is 57.04 $m^2\ g^{-1}$, rather higher than that of Fe_3O_4 materials with other morphologies. This open hollow microstructure of the sample with a large surface area facilitates larger area for the electrolyte contact, resulting in fast Li ion mobility and lower charge-transfer resistance, in return, reducing the local density for a given total current [25].

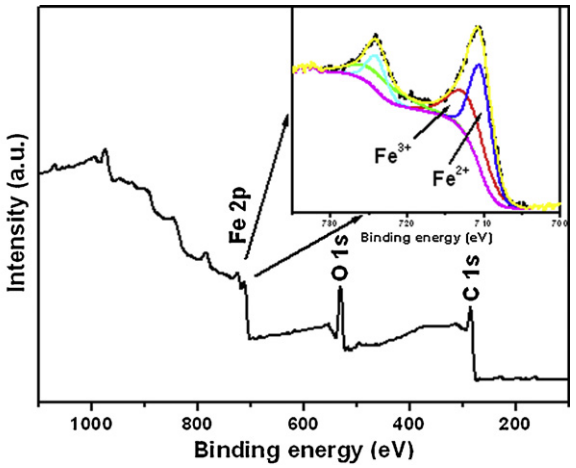

Fig. 4. X-ray photoelectron spectra for Fe_3O_4—C micrometer open hollow sphere the expanded spectra of Fe 2p.

3.3. Electrochemical performance

In order to well understand the performance of the Fe_3O_4—C micrometer open hollow sphere material in lithium ion battery (specific capacity, cyclic stability and rate capability), the

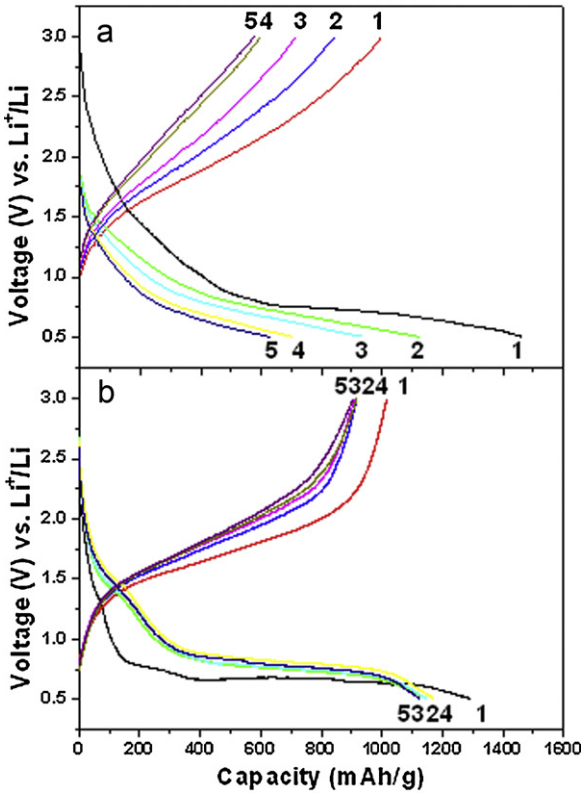

Fig. 6. The discharge/charge profiles of (a) bare Fe_3O_4 particle and (b) Fe_3O_4—C micrometer open hollow sphere in the voltage range 0.5–3.0 V at a current rate of 0.1C.

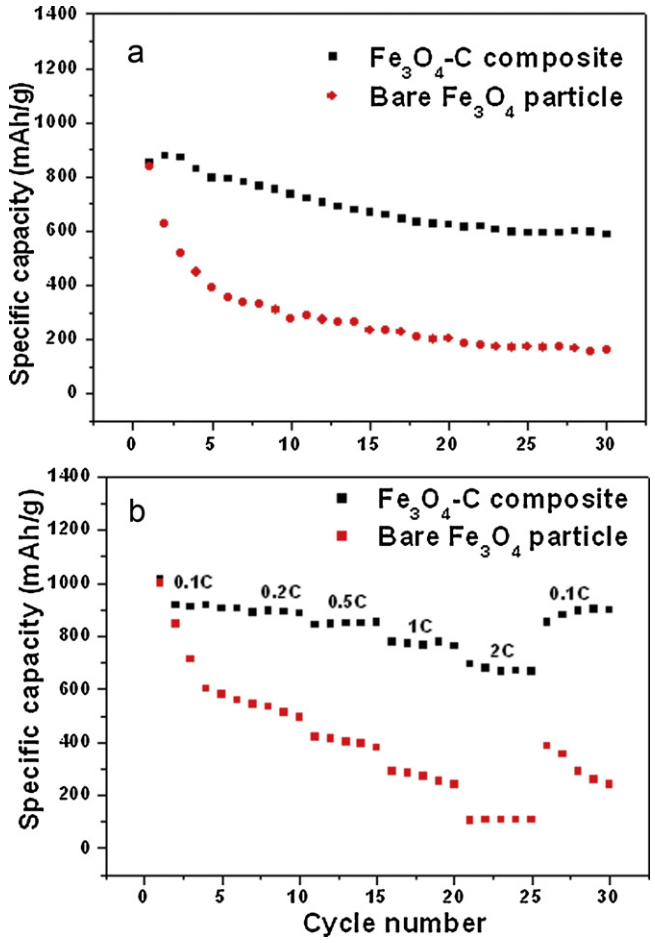

Fig. 7. (a) Cycle and (b) rate performance of bare Fe_3O_4 particle and Fe_3O_4—C micrometer open hollow sphere in the voltage range 0.5–3.0 V at a current rate of 1C.

electrochemical properties with respect to Li insertion/extraction are investigated. The experiments are carried out by using galvanostatic cycling at room temperature in coin cells with metallic lithium as the negative electrode. The electrochemical properties of bare Fe_3O_4 particle with similar morphology (synthesized according to Ref. [26]) are also investigated for comparison.

The first five discharge/charge cycles are tested at a relative low current rate of C/10 (=90 mAh g^{-1}), and the corresponding discharge/charge voltage data are shown in Fig. 6. The first discharge curves of the bare Fe_3O_4 and the as prepared Fe_3O_4—C micrometer open hollow sphere are similar, with a potential plateau at about 0.7 V versus Li^+/Li, which are close to that described in the literature for Fe_3O_4 anodes [27]. During the first five cycles, the specific capacities of the bare Fe_3O_4 particle sample fade quickly in Fig. 6a, indicating of poor cycling performance. While the Fe_3O_4—C open hollow sphere sample shows much better performance, with the first specific charge capacity as high as 1015.9 mAh g^{-1}, and there is no obviously fade in cycle 2 to cycle 5, as seen in Fig. 6b. As reported in Refs. [28,29], the initial discharge capacity calculated on the basis of the whole mass of both samples exceed the theoretical capacity of Fe_3O_4 (928 mAh g^{-1}), which is usually ascribed to the formation of a polymeric gel-like film and possibly interfacial lithium storage.

As shown in Fig. 7a, the cycling performances of Fe_3O_4—C open hollow sphere sample as well as the bare Fe_3O_4—C sample are evaluated between 0.5 and 3.0 V versus Li^+/Li at the charge/discharge current of 1C. During the first 5 cycles, it was found that the capacity of the bare Fe_3O_4—C sample fade to 390 mAh g^{-1} from 837.4 mAh g^{-1} immediately and then decreased to 163.6 mAh g^{-1} after 30 discharge/charge cycles. While the capacity of the Fe_3O_4—C open hollow sphere sample also decreased but remained 587.4 mAh g^{-1}, which is 3.6 times of that of the bare Fe_3O_4—C sample and also much higher than that of above-mentioned references. Fig. 7b shows the rate performance of Fe_3O_4—C open hollow sphere and the bare Fe_3O_4—C samples. During the experiments, the samples were charged/discharged at different C-rates. For each discharge rate of 0.1C, 0.2C, 0.5C, 1C, and 2C, the discharge capacities of the first cycle are obtained as 849.3, 793.8, 719.1, 659.5, and 613.6 mAh g^{-1}, respectively. Compared with these data of the bare Fe_3O_4—C sample and above-mentioned references, the rate performance of the Fe_3O_4—C open hollow sphere sample is greatly enhanced. When the current rate is again reduced back to 0.1C, the capacity just shows a low initial capacity 857.4 mAh g^{-1}, then increases to 899.7 mAh g^{-1} gradually. These results clearly show that the carbon coating and the unique morphology in Fe_3O_4—C open hollow sphere sample plays an important role in improving the rate capability. The native carbon not only improves the local conductivity but also prevents the detachment and aggregation of possibly pulverized Fe_3O_4 nanoparticles during cycling. And the unique morphology as open hollow sphere is helpful to reduce local current density and provide buffer space. Base on these factors mentioned above, the properties of Fe_3O_4—C open hollow sphere as lithium ion battery anode material are greatly enhanced.

4. Conclusions

In summary, we report a solvothermal method and further carbothermal process to fabricate sub-micrometer Fe_3O_4—C material used as lithium ion battery anode. The as-obtained sample has the hierarchical morphology as open hollow sphere self-assembled by carbon-coating Fe_3O_4 nanocrystals. Due to the unique nano/micro hierarchical structure, carbon coating and space buffer effect, the Fe_3O_4—C sample exhibits high capacity, good cycle stability and enhanced rate capability compared with bare Fe_3O_4 particles. And nano/micro material with carbon coating is a promising method to enhance the performance of transition metal oxides as lithium ion battery anode materials.

Acknowledgments

The authors appreciate the financial support of the National Basic Research Program of China (No. 2009CB220100) and the National High Technology Research and Development Program of China (No. 2009AA035200).

References

[1] K. Ozawa, Solid State Ionics 69 (1994) 212–221.
[2] P. Poizot, S. Laruelle, S. Grugeon, L. Dupont, J.M. Tarascon, Nature 407 (2000) 496–499.
[3] J.M. Tarascon, M. Armand, Nature 414 (2001) 359–367.
[4] L. Wang, Y. Yu, P.C. Chen, D.W. Zhang, C.H. Chen, J. Power Sources 183 (2008) 717–723.
[5] W.M. Zhang, X.L. Wu, J.S. Hu, Y.G. Guo, L.J. Wan, Adv. Funct. Mater. 18 (2008) 3941–3946.
[6] Y. He, L. Huang, J.S. Cai, X.M. Zheng, S.G. Sun, Electrochim. Acta 55 (2010) 1140–1144.
[7] S.L. Jin, H.G. Deng, D.H. Long, X.J. Liu, L.A. Zhan, X.Y. Liang, W.M. Qiao, L.C. Ling, J. Power Sources 196 (2011) 3887–3893.
[8] M.M. Rahman, J.Z. Wang, M.F. Hassan, Z.X. Chen, H.K. Liu, J Alloy Compd. 509 (2011) 5408–5413.
[9] J. Wang, X.M. Liu, H. Yang, X.D. Shen, J Alloy Compd. 509 (2011) 712–718.
[10] S.Q. Wang, J.Y. Zhang, C.H. Chen, J. Power Sources 195 (2010) 5379–5381.
[11] L.Q. Chen, W.P. Liu, J.L. Chen, X.F. Yang, J. Liu, X.H. Fu, M.M. Wu, Sci. China Chem. 54 (2011) 923–929.
[12] M. Nagao, M. Otani, H. Tomita, S. Kanzaki, A. Yamada, R. Kanno, J. Power Sources 196 (2011) 4741–4746.

[13] J.P. Liu, Y.Y. Li, H.J. Fan, Z.H. Zhu, J. Jiang, R.M. Ding, Y.Y. Hu, X.T. Huang, Chem. Mater. 22 (2010) 212–217.
[14] H.N. Duan, J. Gnanaraj, X.P. Chen, B.Q. Li, J.Y. Liang, J. Power Sources 185 (2008) 512–518.
[15] M. Zhang, D. Lei, X. Yin, L. Chen, Q. Li, Y. Wang, T. Wang, J. Mater. Chem. 20 (2010) 5538.
[16] H. Liu, G.X. Wang, J.Z. Wang, D. Wexler, Electrochem. Commun. 10 (2008) 1879–1882.
[17] G.H. Lee, J.G. Park, Y.M. Sung, K.Y. Chung, W. Il Cho, D.W. Kim, Nanotechnology 20 (2009).
[18] T.A. Kandiel, A. Feldhoff, L. Robben, R. Dillert, D.W. Bahnemann, Chem. Mater. 22 (2010) 2050–2060.
[19] S.K. Meher, P. Justin, G.R. Rao, Electrochim. Acta 55 (2010) 8388–8396.
[20] C.S. Riccardi, R.C. Lima, M.L. dos Santos, P.R. Bueno, J.A. Varela, E. Longo, Solid State Ionics 180 (2009) 288–291.
[21] W.D. Zhang, H.M. Xiao, L.P. Zhu, S.Y. Fu, J Alloy Compd. 477 (2009) 736–738.
[22] Y.C. Chang, D.H. Chen, J. Colloid Interface Sci. 283 (2005) 446–451.
[23] P.C.J. Graat, M.A.J. Somers, Appl. Surf. Sci. 100 (1996) 36–40.
[24] D.H.E.K.S.W. Sing, R.A.W. Haul, L. Moscou, R.A. Pierotti, J. Rouquerol, T. Siemieniewska, Appl. Chem. 57 (1985).
[25] C.W. Sun, S. Rajasekhara, J.B. Goodenough, F. Zhou, J. Am. Chem. Soc. 133 (2011) 2132–2135.
[26] L.P. Zhu, H.M. Xiao, W.D. Zhang, G. Yang, S.Y. Fu, Cryst. Growth Des. 8 (2008) 957–963.
[27] I.A. Courtney, J.R. Dahn, J. Electrochem. Soc. 144 (1997) 2045–2052.
[28] S.L. Chou, J.Z. Wang, D. Wexler, K. Konstantinov, C. Zhong, H.K. Liu, S.X. Dou, J. Mater. Chem. 20 (2010) 2092–2098.
[29] X.L. Wu, Y.G. Guo, L.J. Wan, C.W. Hu, J. Phys. Chem. C 112 (2008) 16824–16829.